

Supporting Information

Distinction of Mechanisms Causing Experimental Degradation of Perovskite Solar Cells by Simulating Associated Pathways

Arthur Julien,* Jean-Baptiste Puel and Jean-François Guillemoles

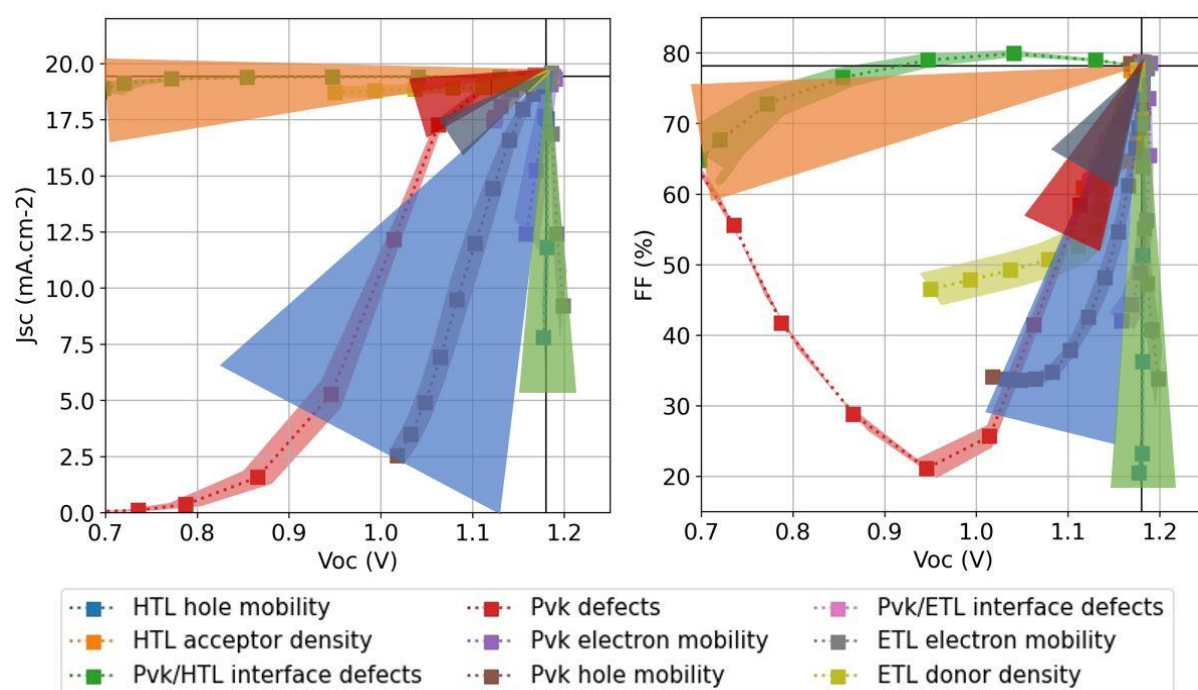


Figure S1. Degradation pathways of simulated mechanisms in J_{sc}/V_{oc} and FF/V_{oc} planes (squares and dotted lines). Shaded areas show the trends depicted in Table 1. Blue correspond to the decomposition of perovskite material, orange to the reaction with metal electrodes, green to the thermal instability of HTL, red to the oxidation of HTL, and black to the photocatalytic effect of ETL.

Table S1. Definition of devices reproduced through reported initial performances and materials. Material parameters reported here are taken from literature, others in the ranges defined in Table S2.

Source for perovskite solar cell	Peng <i>et al.</i> ¹	Li <i>et al.</i> ²		Chen <i>et al.</i> ³	Lim <i>et al.</i> ⁴		
		MPP	Voc		40 °C	55 °C	70 °C
Voc (V)	1.18	1.079	1.092	1.09	1.027	1.012	1.042
Jsc (mA.cm-2)	19.41	22.77	22.89	15.65	22.29	23.34	23.16
FF (%)	78.0	76.31	77.12	72.0	59.77	62.39	57.39
Structure	nip	nip		pin	nip		
Perovskite material	CS _{0.05} FA _{0.88} MA _{0.07} PbI _{2.56} Br _{0.44}	FA _{0.9} CS _{0.1} PbI ₃		CS _{0.7} FA _{0.3} PbI ₂ Br	FA _{0.95} MA _{0.05} PbI _{2.85} Br _{0.15}		
Bandgap (eV)	1.62 ¹	1.51 ⁵		1.82 ³	1.62 ⁶		
Electron affinity (eV)	3.9 ¹	3.95 ⁵		3.92 ³	3.83 ⁶		
Relative permittivity	64 ¹	64 ¹		64 ¹	64 ¹		
CB effective density of states (eV)	1.00E+19 ¹	1.00E+19 ¹		1.00E+19 ¹	1.00E+19 ¹		
VB effective density of states (eV)	1.00E+19 ¹	1.00E+19 ¹		1.00E+19 ¹	1.00E+19 ¹		
HTL material	spiro-OMeTAD	spiro-OMeTAD / PTAA		NiOx	spiro-OMeTAD		
Bandgap (eV)	3 ⁷	2.98		3.64 ⁸	3 ⁷		
Electron affinity (eV)	2.2 ⁷	2.22 ⁹		1.85 ⁸	2.2 ⁷		
Relative permittivity	3 ⁷	3 ⁷		11.75 ⁸	3 ⁷		
CB effective density of states (eV)	1.00E+20 ⁷	2.00E+18 ⁹		2.50E+20 ⁸	1.00E+20 ⁷		
VB effective density of states (eV)	1.00E+20 ⁷	1.00E+20 ⁷		2.50E+20 ⁸	1.00E+20 ⁷		
ETL material	TiO2	SnO2		C60	SnO2		
Bandgap (eV)	3.2 ¹⁰	3.5 ¹¹		1.7 ¹⁰	3.5 ¹¹		
Electron affinity (eV)	3.9 ¹⁰	4 ¹¹		3.9 ¹⁰	4 ¹¹		
Relative permittivity	9 ¹⁰	9 ¹¹		4.2 ¹⁰	9 ¹¹		
CB effective density of states (eV)	1.00E+19 ¹⁰	2.20E+17 ¹¹		8.00E+19 ¹⁰	2.20E+17 ¹¹		
VB effective density of states (eV)	1.00E+19 ¹⁰	2.20E+17 ¹¹		8.00E+19 ¹⁰	2.20E+17 ¹¹		

Table S2. Material parameters defined through randomized procedure and authorized ranges established from literature.

	Minimum value	Maximum value
HTL hole mobility (cm ² .V ⁻¹ .s ⁻¹)	1.00E-02	1.00E+00
HTL acceptor density (cm ⁻³)	1.00E+15	2.00E+18
HTL/pvk interface defects (cm ⁻²)	1.00E+10	1.00E+18
Pvk electron mobility (cm ² .V ⁻¹ .s ⁻¹)	1.00E-01	1.00E+01
Pvk hole mobility (cm ² .V ⁻¹ .s ⁻¹)	1.00E-01	1.00E+01
Pvk defect density (cm ⁻³)	1.00E+10	1.00E+18
ETL/pvk interface defects (cm ⁻²)	1.00E+10	1.00E+18
ETL electron mobility (cm ² .V ⁻¹ .s ⁻¹)	1.00E-02	1.00E+00
ETL donor density (cm ⁻³)	1.00E+16	1.00E+19

Genetic algorithm to reproduce initial JV performances of a given solar cell

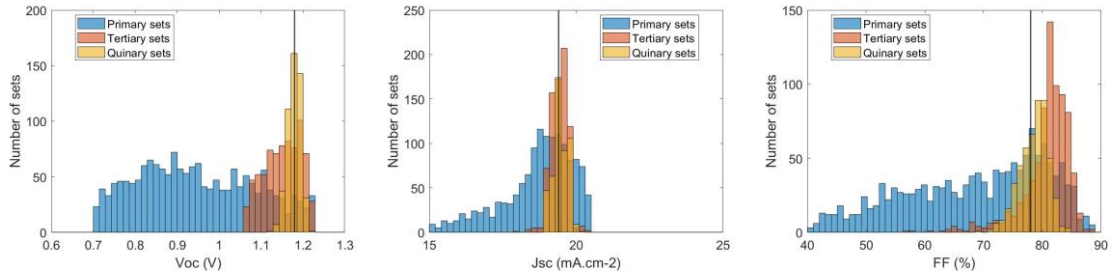
Along the whole procedure, material parameters defined in Table S1 are considered as known, and parameters listed in Table S2 are varied to match Voc, Jsc and FF values experimentally measured. Six steps are implemented to obtain a sufficiently large set of simulations reproducing sufficiently closely the experimental values :

1. Random generation: Material parameters are randomly picked in the ranges defined in Table S2. A log-uniform distribution is used. For each device studied here, 2000 sets and associated drift diffusion simulations are performed.
2. Selection: JV curves having Voc, Jsc and FF values within $\pm 5\%$ range are selected. Table S3 reports the number of selected sets for each studied device.
3. Mutation: Varied material parameters from the sets previously selected are modified. To do so, they are multiplied by a coefficient randomly picked between 1/5 and 5. Here a log-uniform distribution is also used. For each device studied here, 750 sets are generated, and associated drift diffusion simulations are performed.
4. Selection: JV curves having Voc, Jsc and FF values within $\pm 3\%$ range are selected. Table S3 reports the number of selected sets for each studied device.
5. Mutation: The same procedure as in step three is used. Here material parameters are modified by a ratio between 1/2 and 2.
6. Selection: JV curves having Voc, Jsc and FF values within $\pm 2\%$ range are selected. Table S3 reports the number of selected sets for each studied device.

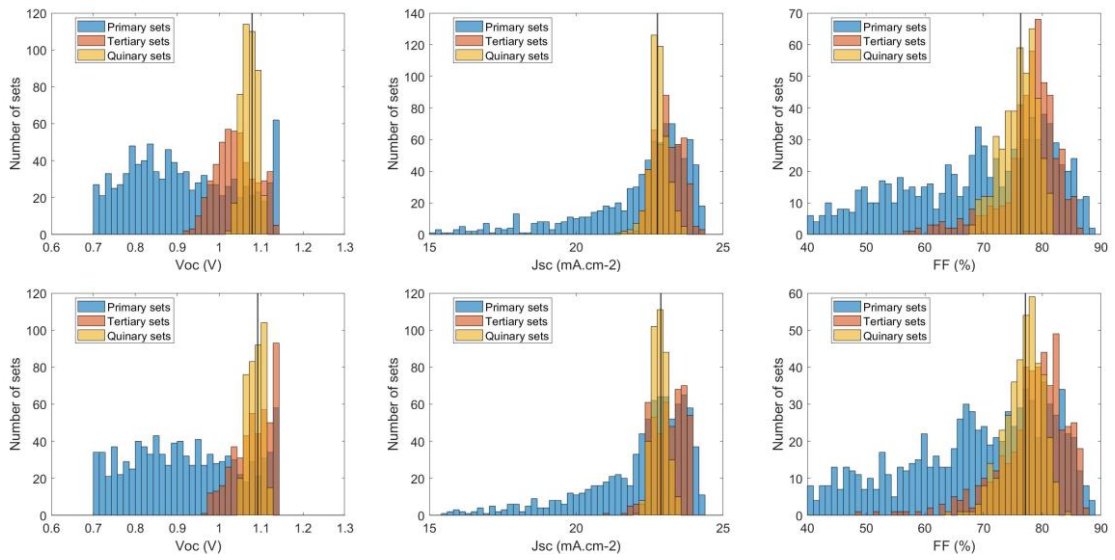
Table S3. Number of selected sets at each step in the genetic algorithm procedure.

	Selected sets in second step ($\pm 5\%$ error)	Selected sets in fourth step ($\pm 3\%$ error)	Selected sets in sixth step ($\pm 2\%$ error)
Peng et al. (spiro-OMeTAD HTL)	39	41	98
Peng et al. (P3HT:CuPc HTL)	83	108	108
Li et al. (MPP)	41	14	104
Li et al. (Voc)	65	18	125
Chen et al.	47	56	107
Lim et al. (40 °C)	36	23	101
Lim et al. (55 °C)	32	37	109
Lim et al. (70 °C)	14	45	49
Lim et al. (40 °C – second part)	16	25	72
Lim et al. (55 °C – second part)	14	13	74
Lim et al. (70 °C – second part)	10	10	87

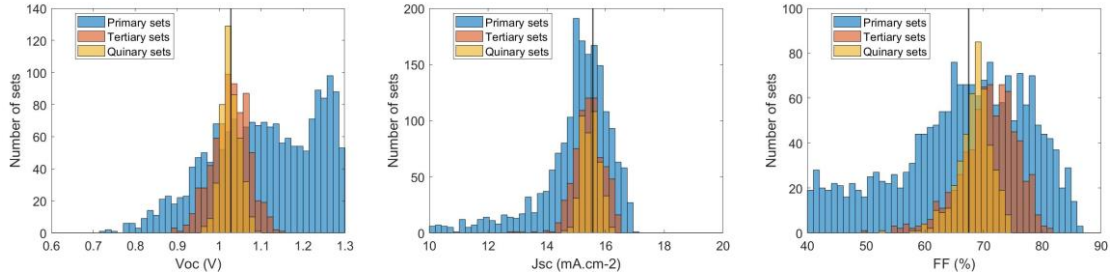
Peng et al.



Li et al. (top: MPP, bottom: Voc)



Chen et al.



Lim et al. (top: 40 °C, middle : 55 °C, bottom: 70 °C)

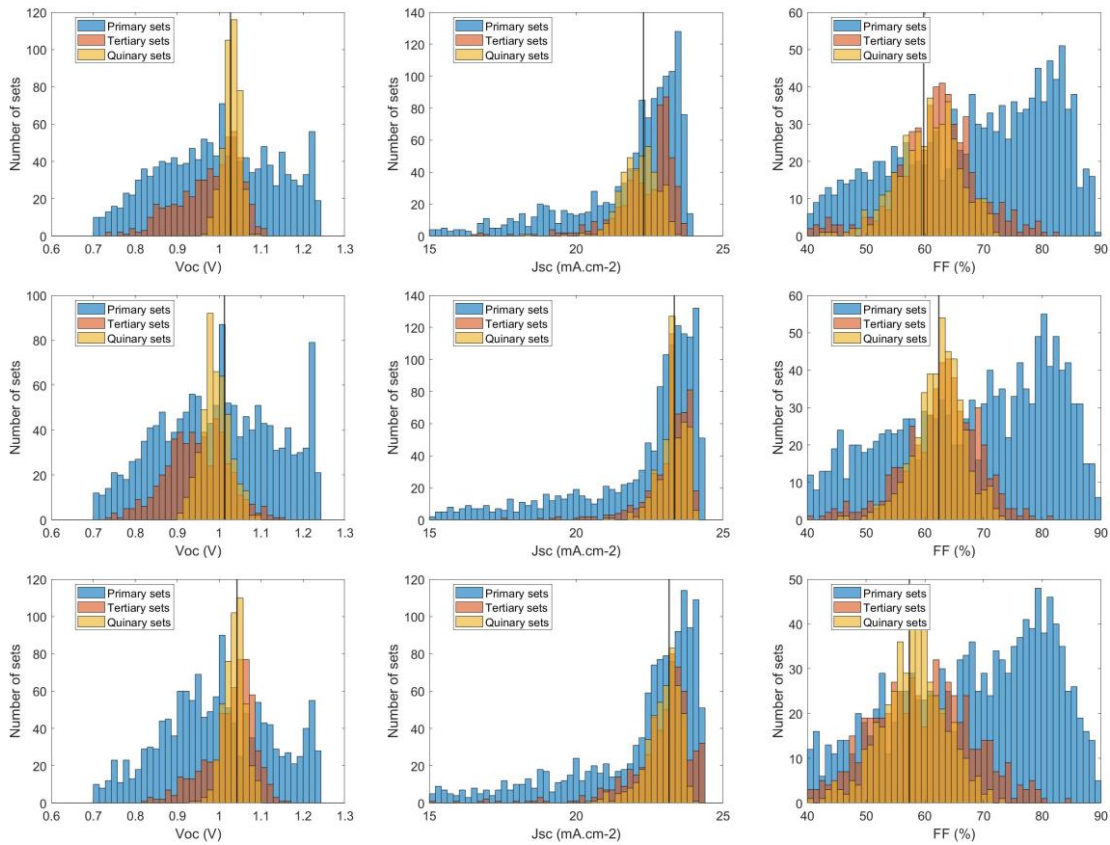
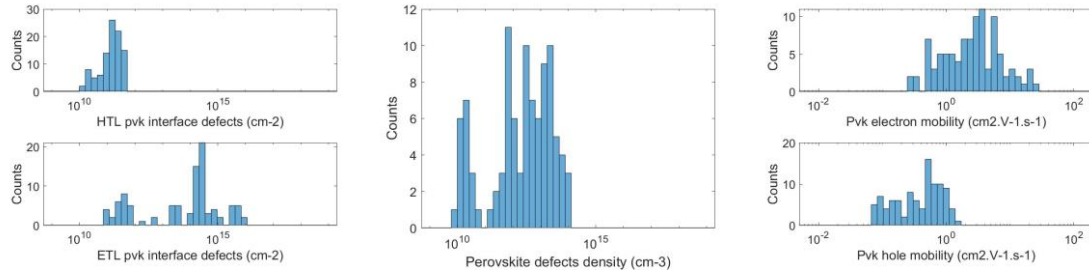
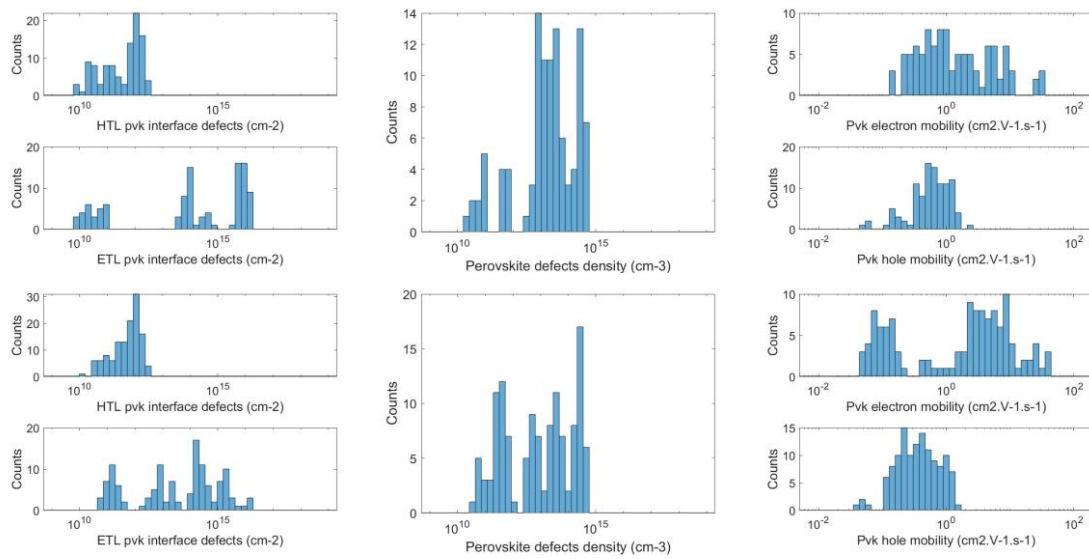


Figure S2. Statistics of Voc, Jsc and FF associated to material parameters sets obtained along selection procedure. Primary sets are the first initially generated, tertiary and quinary sets are obtained after the first and second perturbation steps respectively. Vertical lines show the experimental value.

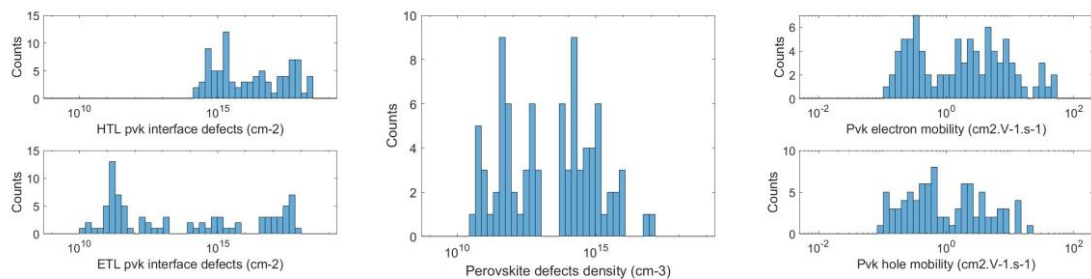
Peng et al.



Li et al. (top: MPP, bottom: Voc)



Chen et al.



Lim et al. (top: 40 °C, middle : 55 °C, bottom: 70 °C)

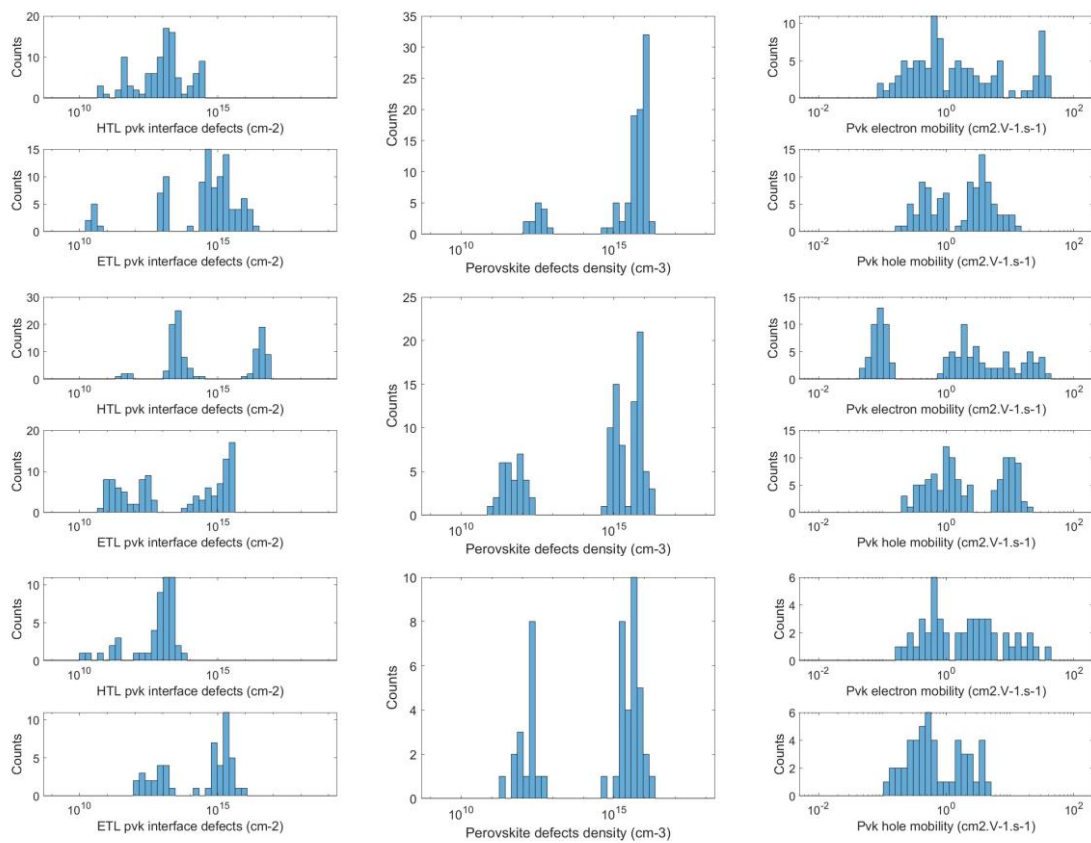
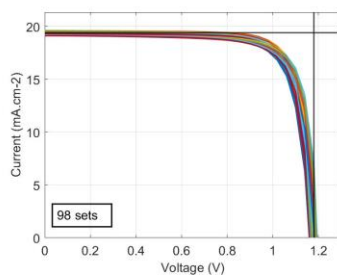
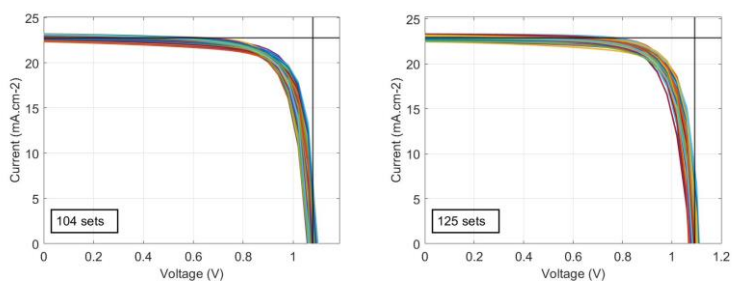


Figure S3. Statistics of interface or bulk defect densities, and carrier mobilities in perovskite layer in the group obtained after the final selection step. This final group reproduces experimental performances, with a statistical approach.

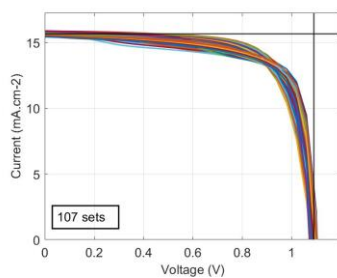
Peng et al.



Li et al. (left: MPP, right : Voc)



Chen et al.



Lim et al. (left 40°C, middle : 55 °C, right: 70 °C)

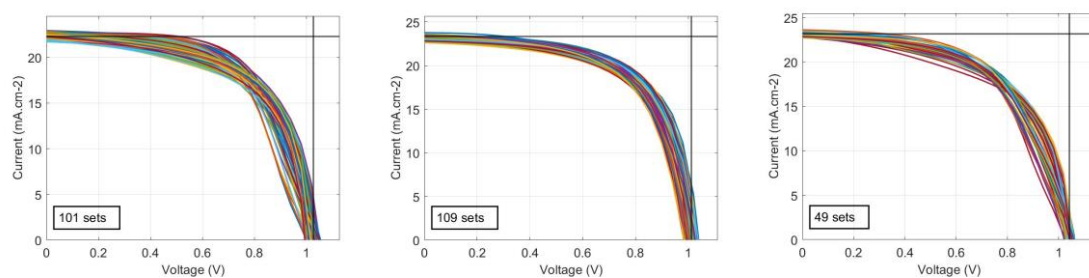
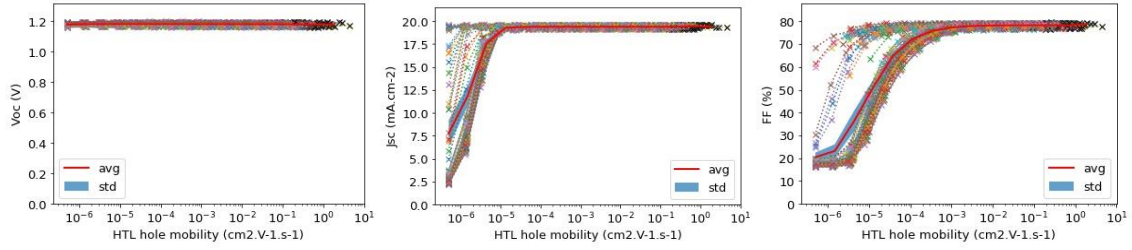
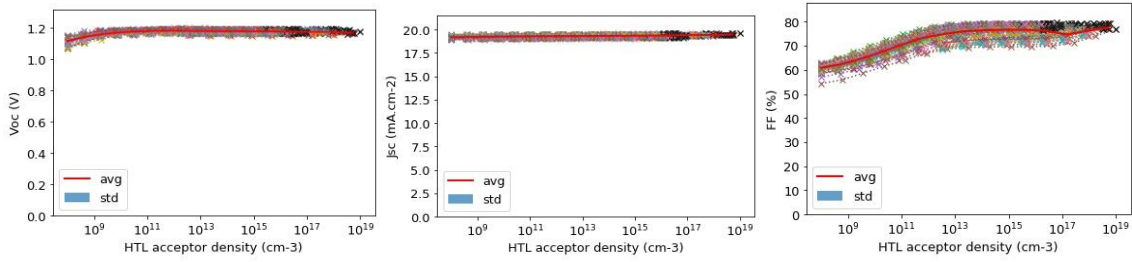


Figure S4. JV curves reproducing initial performances of studied devices. Box displays the number of sets / JV curves.

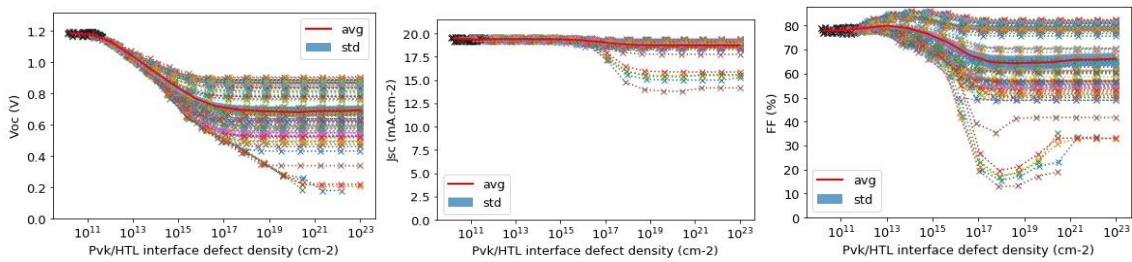
Decrease of hole mobility in HTL



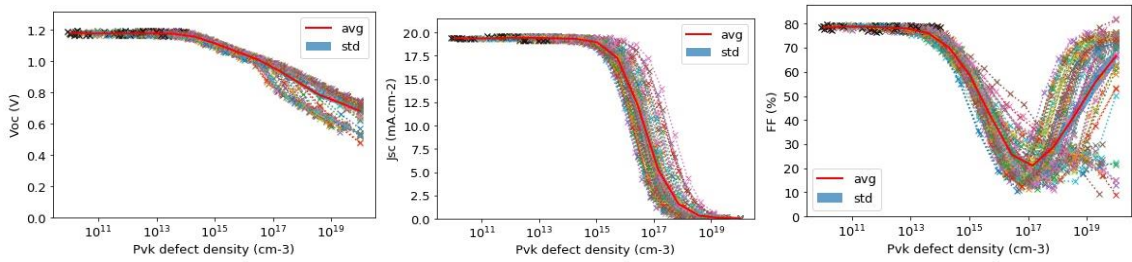
Decrease of doping in HTL



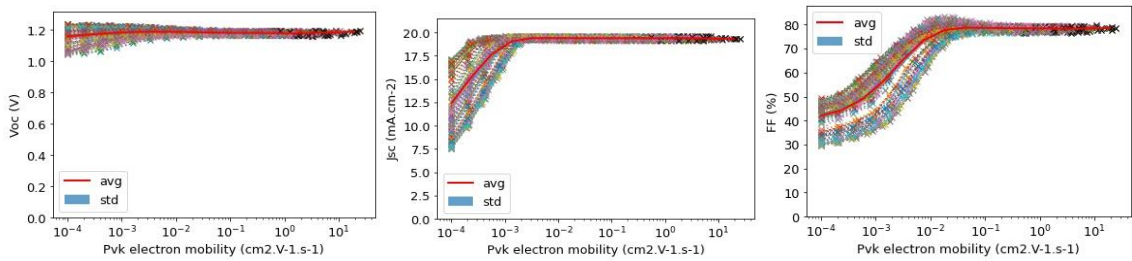
Increase of defect density at HTL/perovskite interface



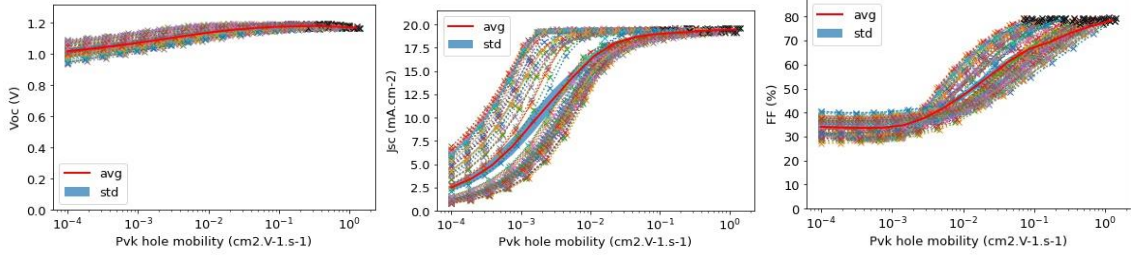
Increase of defect density in perovskite



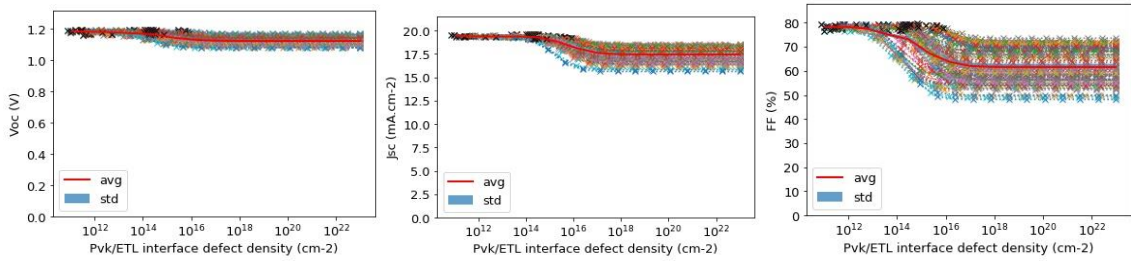
Decrease of electron mobility in perovskite



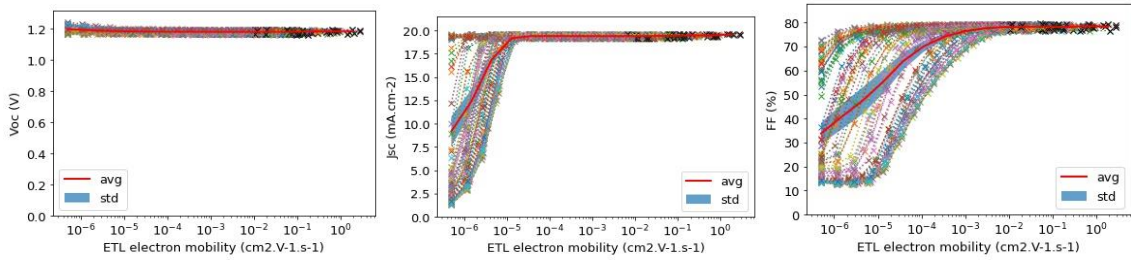
Decrease of hole mobility in perovskite



Increase of defect density at ETL/perovskite interface



Decrease of electron mobility in ETL



Decrease of doping in ETL

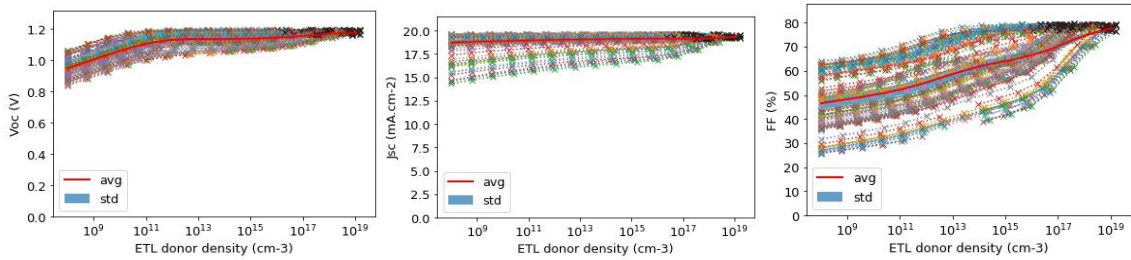
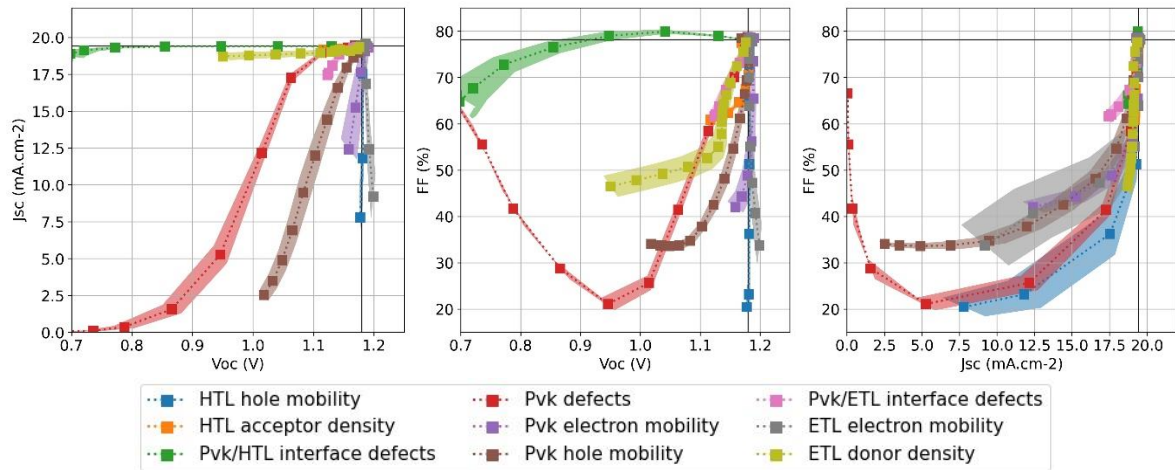
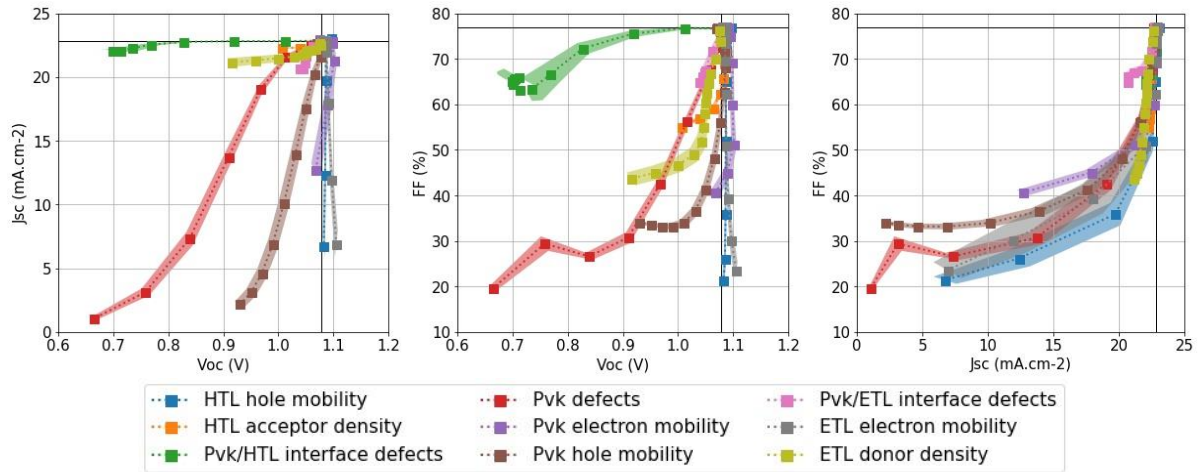


Figure S5. Evolution of Voc, Jsc and FF for implemented degradation mechanisms. The response of each material parameters set is represented (98 in this example, all reproducing the initial performance of devices studied by Peng *et al.*). The clear similarity of evolutions allows to compute an average behavior (red line) and 95 % confidence interval (shaded area).

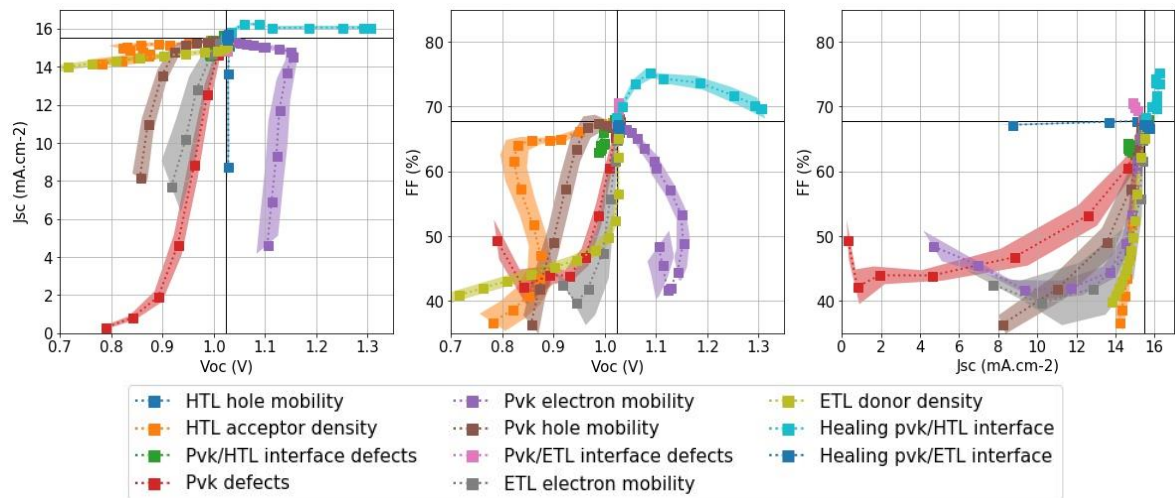
Peng et al.



Li et al. (top : MPP, bottom : Voc)



Chen et al.



Lim et al. (top: 40 °C, middle: 55 °C, bottom: 70 °C)

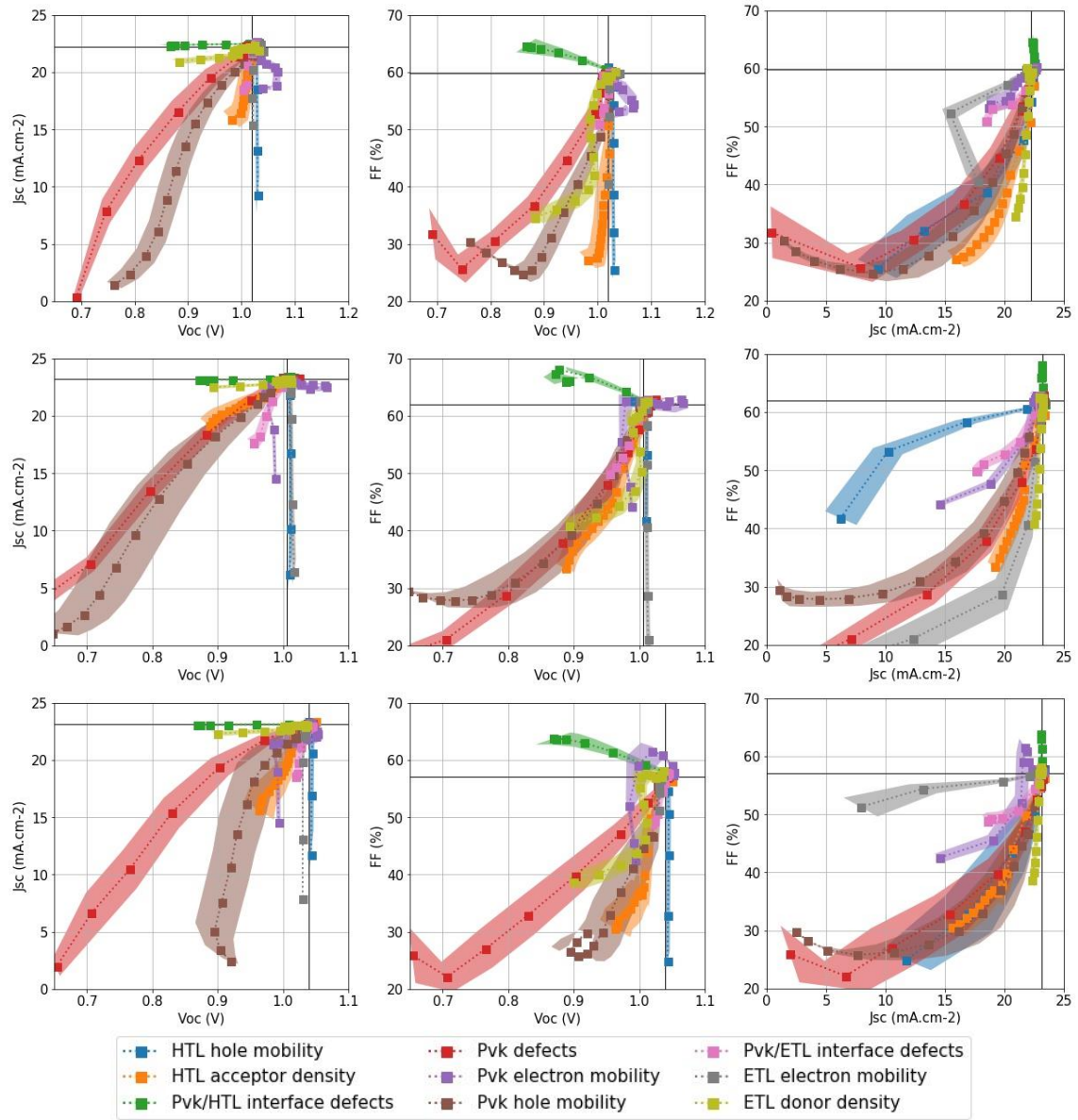
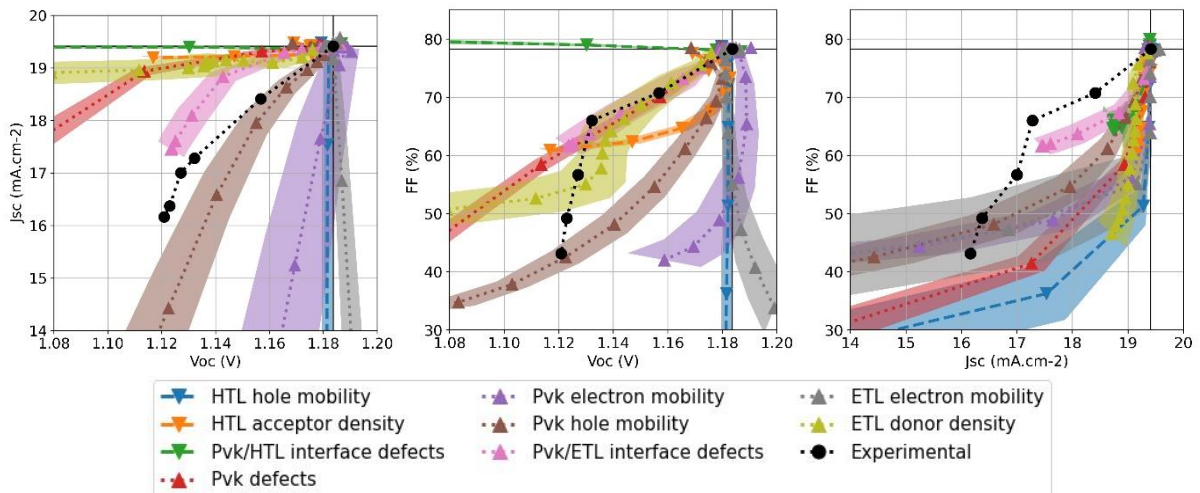
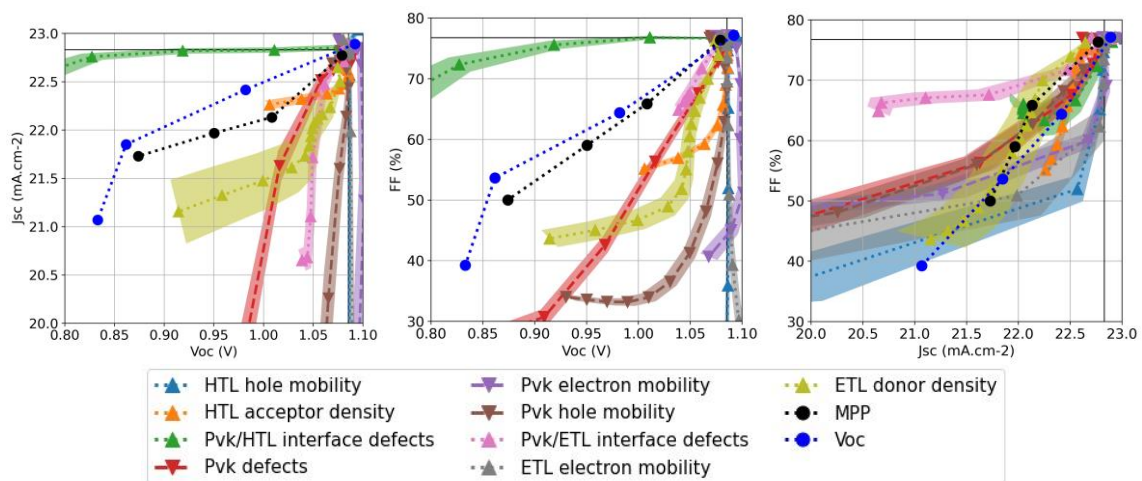


Figure S6. Degradation pathways of simulated mechanisms in J_{sc}/V_{oc} , FF/V_{oc} and FF/J_{sc} planes. Average value is represented with squares and dotted lines, shaded areas represent the 95 % confidence interval.

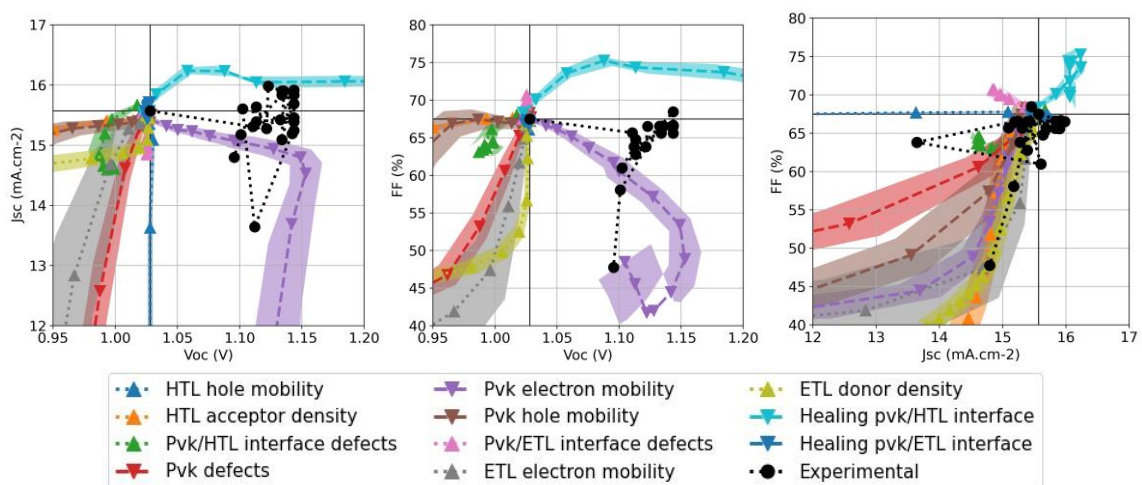
Peng et al.



Li et al.



Chen et al.



Lim et al. (top: 40 °C, middle: 55 °C, bottom: 70 °C)

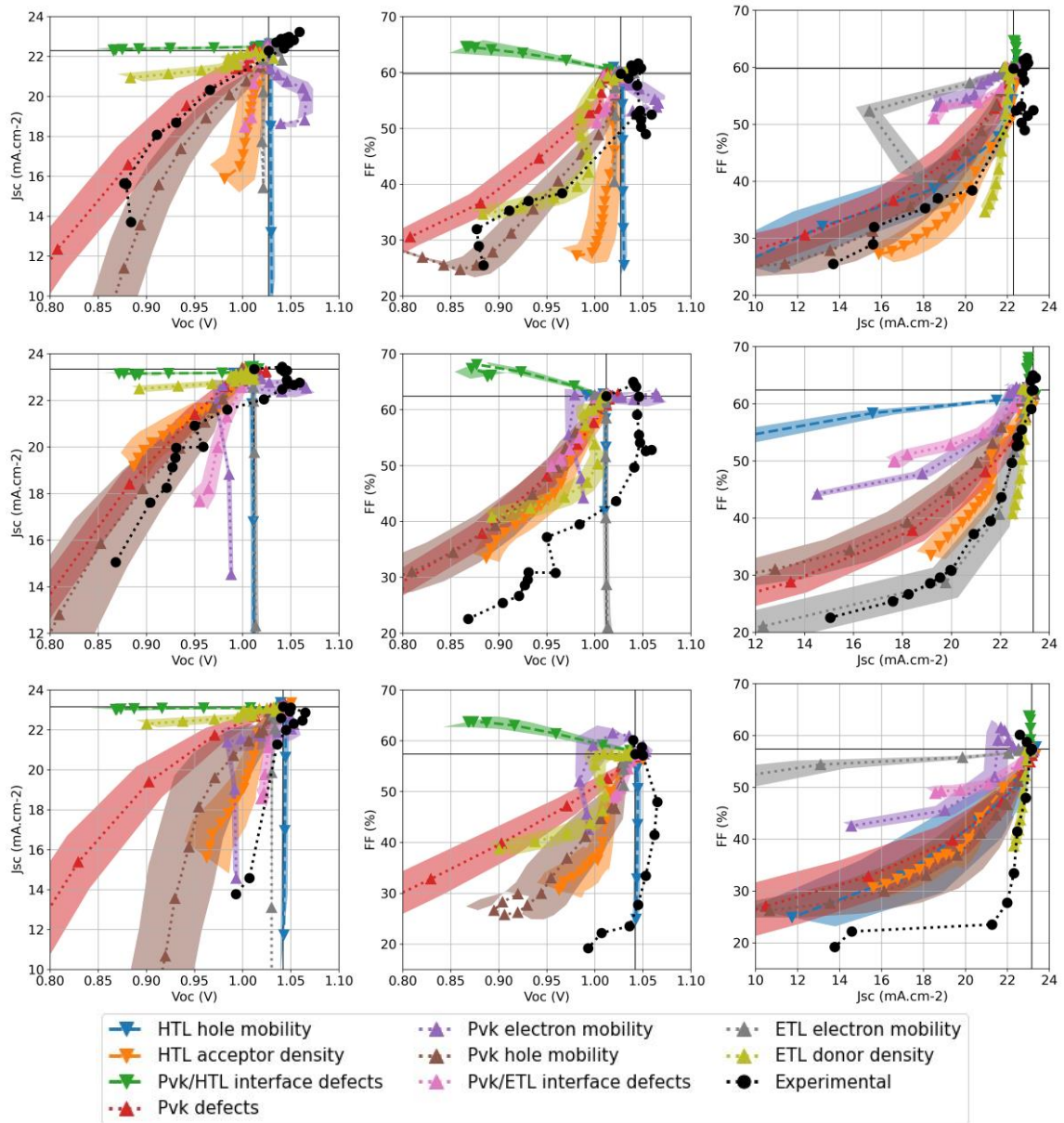


Figure S7. Experimental degradation pathways in J_{sc}/V_{oc} , FF/V_{oc} and FF/J_{sc} planes. Associated simulated pathways are superposed (down triangles and dashed lines for causes identified by authors, up triangles and dotted lines for others).

Table S4. Definition of devices studied by Peng *et al.* with P3HT:CuPc HTL, reproduced through reported initial performances and materials. Material parameters reported here are taken from literature, others in the ranged defined in Table S2.

Source for perovskite solar cell	Peng et al.
Voc (V)	1.19
Jsc (mA.cm-2)	19.80
FF (%)	81.0
Structure	nip
Perovskite material	$\text{Cs}_{0.05}\text{FA}_{0.88}\text{MA}_{0.07}\text{PbI}_{2.56}\text{Br}_{0.44}$
Bandgap (eV)	1.62 ¹
Electron affinity (eV)	3.9 ¹
Relative permittivity	64 ¹
CB effective density of states (eV)	1.00E+19 ¹
VB effective density of states (eV)	1.00E+19 ¹
HTL material	P3HT:CuPc
Bandgap (eV)	2.2 ¹
Electron affinity (eV)	3.1 ¹
Relative permittivity	3 ¹
CB effective density of states (eV)	1.00E+20 ¹
VB effective density of states (eV)	1.00E+20 ¹
ETL material	TiO2
Bandgap (eV)	3.2 ¹⁰
Electron affinity (eV)	3.9 ¹⁰
Relative permittivity	9 ¹⁰
CB effective density of states (eV)	1.00E+19 ¹⁰
VB effective density of states (eV)	1.00E+19 ¹⁰

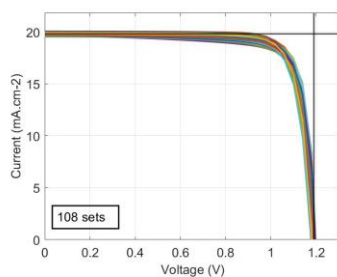


Figure S8. JV curves reproducing initial performances of device studied by Peng *et al.* with P3HT:CuPc HTL

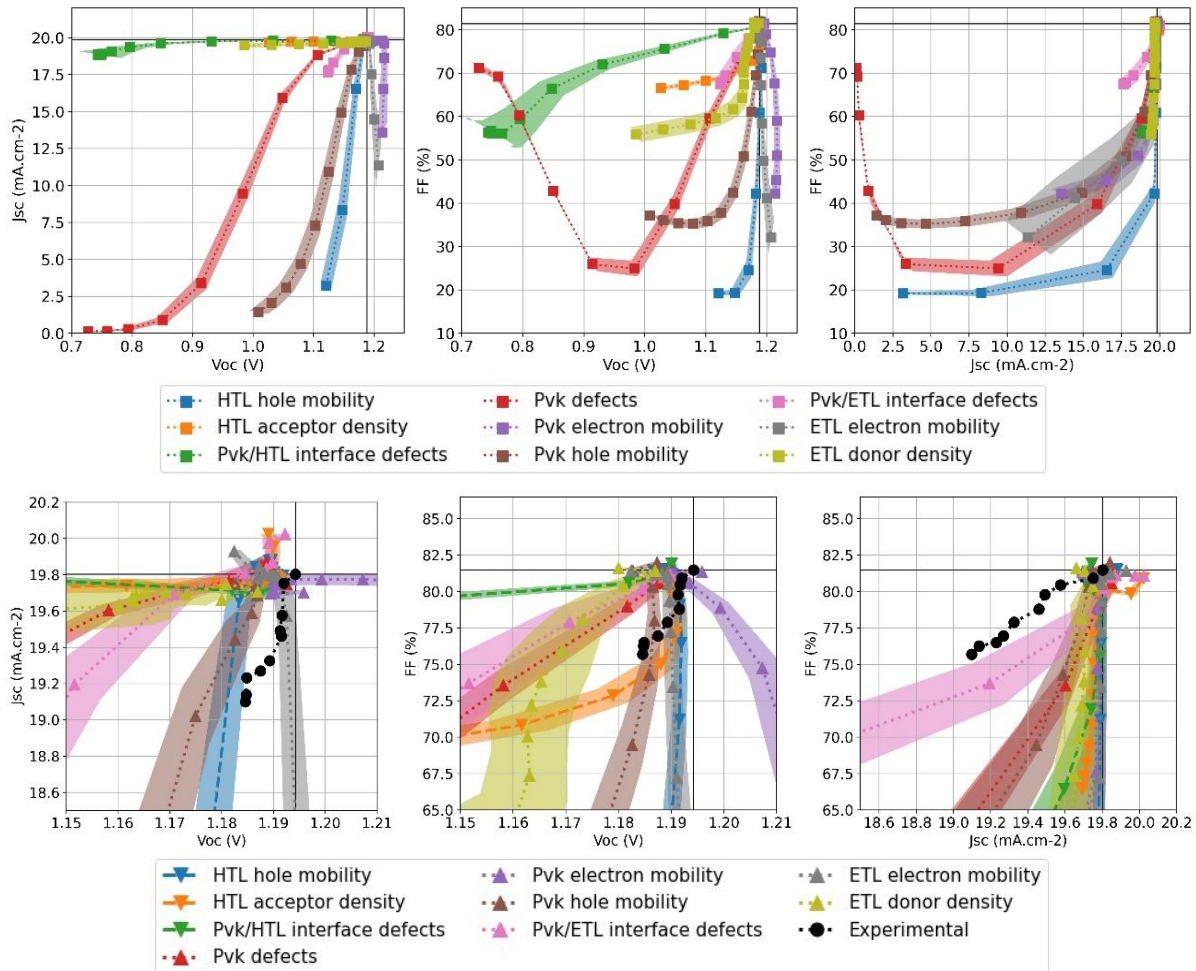


Figure S9. Top: Degradation pathways of simulated mechanisms in J_{sc}/V_{oc} , FF/V_{oc} and FF/J_{sc} planes for devices studied by Peng *et al.* with P3HT:CuPc HTL. Average value is represented with squares and dashed lines, shaded areas represent the 95 % confidence interval. Bottom: Experimental data is superposed, perovskite devices (with P3HT:CuPc HTL) were aged dark, at 85 °C and 85 % RH.

Lim et al. (top: 40 °C, middle: 55 °C, bottom: 70 °C)

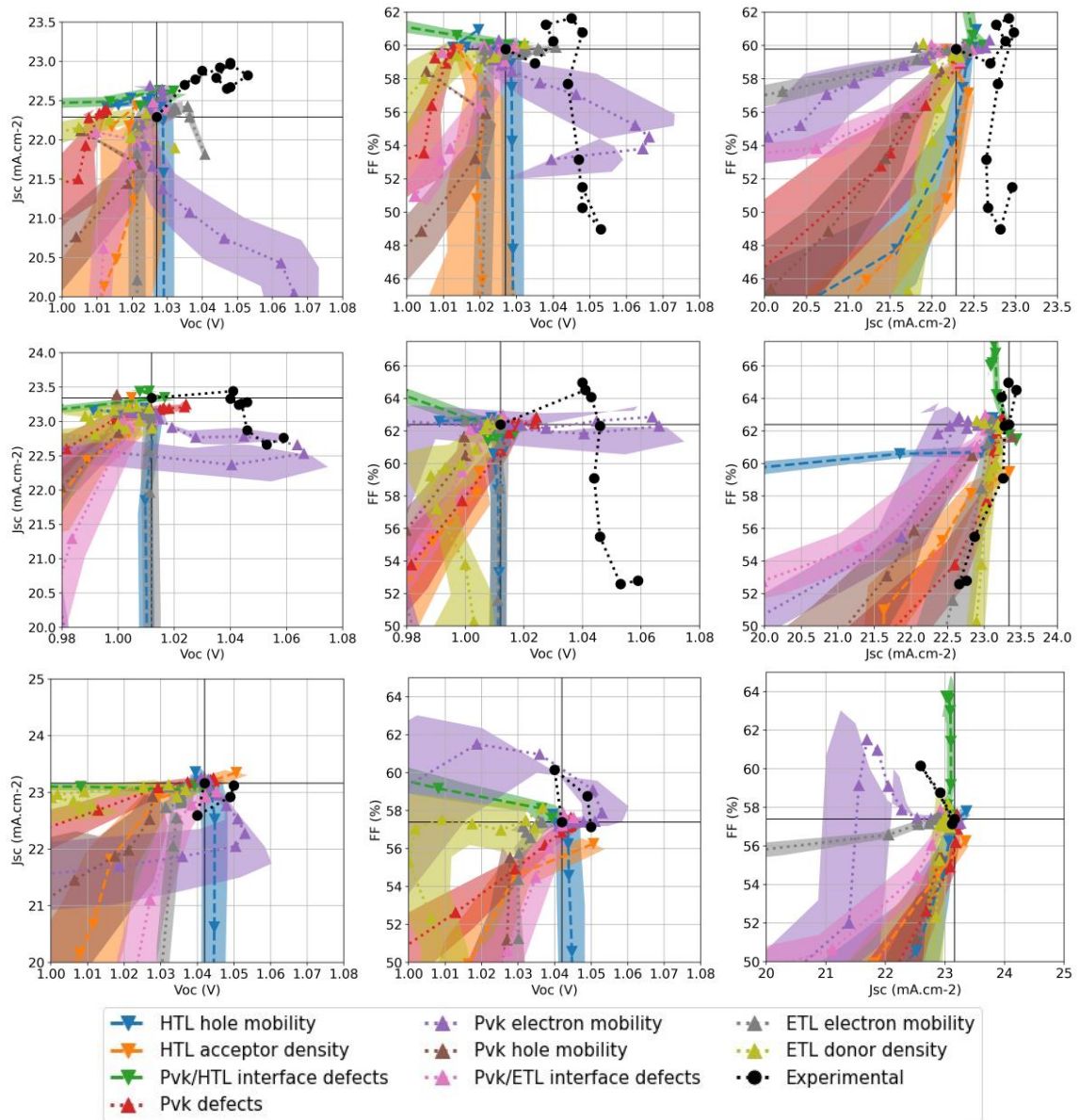


Figure S10. First part of experimental degradation pathways from results published by Lim *et al.* Associated simulated pathways are superposed (down triangles and dashed lines for causes identified by authors, up triangles and dotted lines for others). Top: 40 °C, middle: 55 °C, bottom: 70 °C.

Table S5. Definition of hypothetical devices used to study the second degradation step of results reported by Lim *et al.* They are defined through performances reached at the end of the first degradation step. Material parameters reported here are taken from literature, others in the ranged defined in Table S2.

Source for perovskite solar cell	Lim et al.		
	40 °C	55 °C	70 °C
Voc (V)	1.059	1.047	1.065
Jsc (mA.cm-2)	23.23	22.7	22.87
FF (%)	52.44	54.07	47.95
Structure	nip		
Perovskite material	FA _{0.95} MA _{0.05} PbI _{2.85} Br _{0.15}		
Bandgap (eV)	1.62 ⁶		
Electron affinity (eV)	3.83 ⁶		
Relative permittivity	64 ¹		
CB effective density of states (eV)	1.00E+19 ¹		
VB effective density of states (eV)	1.00E+19 ¹		
HTL material	spiro-OMeTAD		
Bandgap (eV)	3 ⁷		
Electron affinity (eV)	2.2 ⁷		
Relative permittivity	3 ⁷		
CB effective density of states (eV)	1.00E+20 ⁷		
VB effective density of states (eV)	1.00E+20 ⁷		
ETL material	SnO ₂		
Bandgap (eV)	3.5 ¹¹		
Electron affinity (eV)	4 ¹¹		
Relative permittivity	9 ¹¹		
CB effective density of states (eV)	2.20E+17 ¹¹		
VB effective density of states (eV)	2.20E+17 ¹¹		

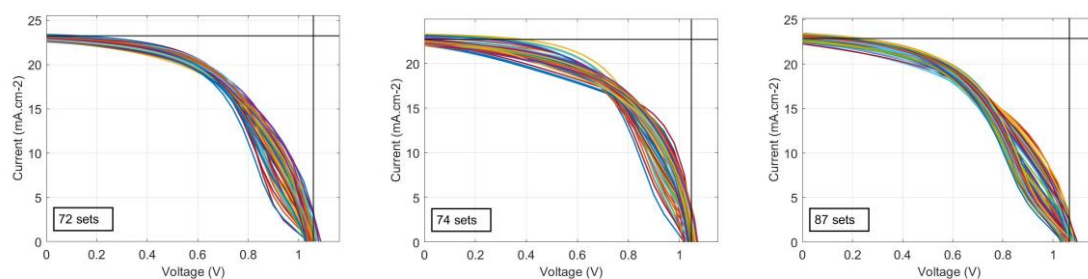
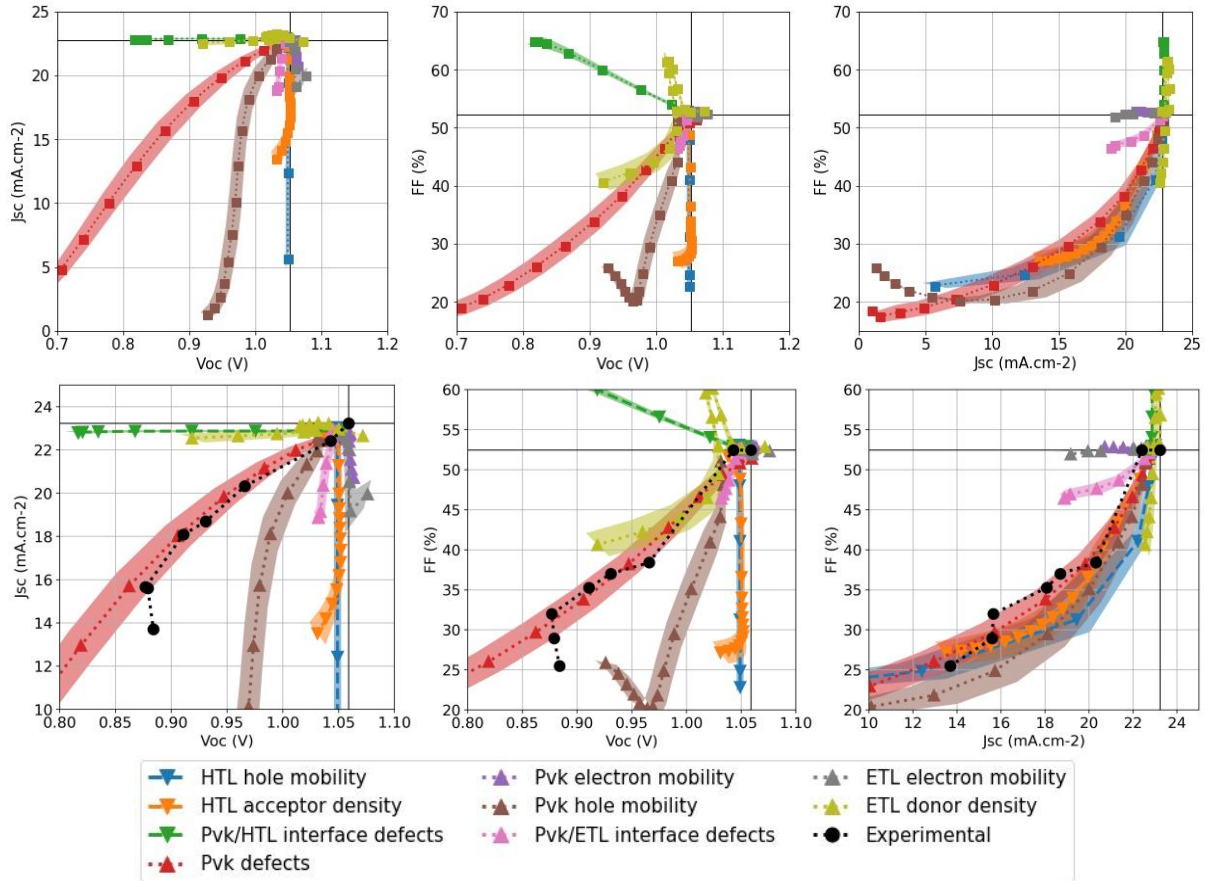
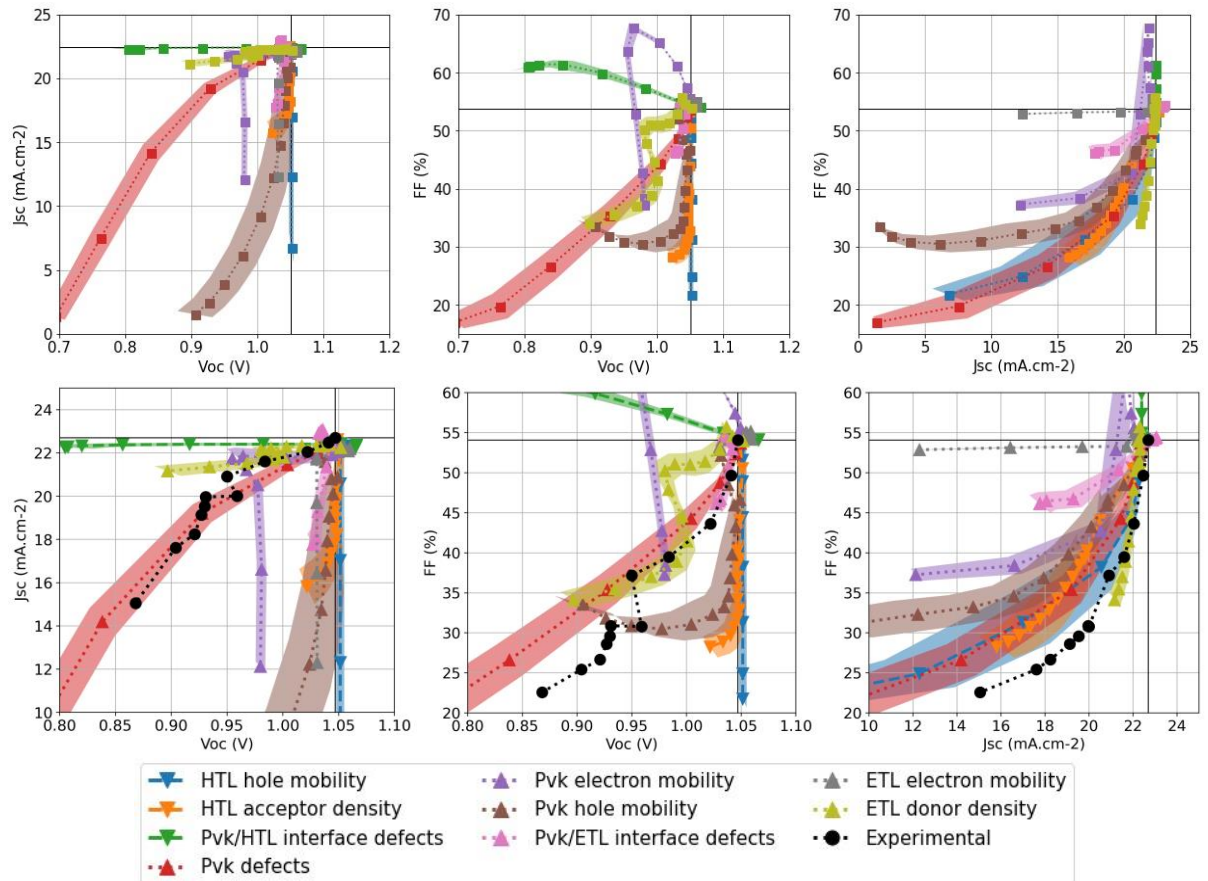


Figure S11. JV curves reproducing performances of hypothetical devices used to study the second degradation step of results reported by Lim *et al.* Left: 40 °C, middle: 55 °C, right: 70 °C.

40 °C



55 °C



70 °C

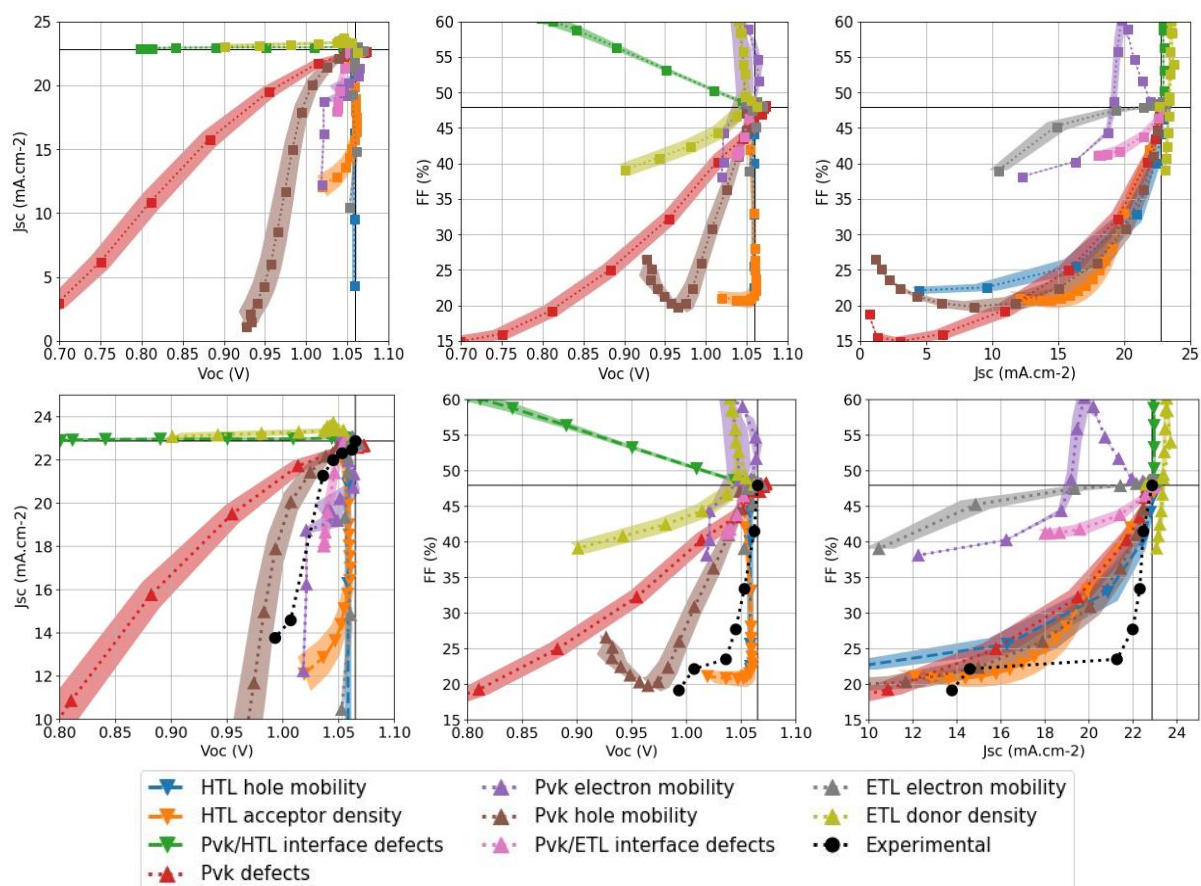


Figure S12. Degradation pathways of simulated mechanisms in J_{sc}/V_{oc} , FF/V_{oc} and FF/J_{sc} planes for hypothetical devices used to study the second degradation step of results reported by Lim *et al.* Average value is represented with squares and dashed lines, shaded areas represent the 95 % confidence interval. Second part of experimental degradation is superposed in a second line for each aging condition.

References

- 1 J. Peng, D. Walter, Y. Ren, M. Tebyetekerwa, Y. Wu, T. Duong, Q. Lin, J. Li, T. Lu, M. A. Mahmud, O. L. C. Lem, S. Zhao, W. Liu, Y. Liu, H. Shen, L. Li, F. Kremer, H. T. Nguyen, D. Y. Choi, K. J. Weber, K. R. Catchpole and T. P. White, *Science (80-.)*, 2021, **371**, 390–395.
- 2 N. Li, Y. Luo, Z. Chen, X. Niu, X. Zhang, J. Lu, R. Kumar, J. Jiang, H. Liu, X. Guo, B. Lai, G. Brocks, Q. Chen, S. Tao, P. David and H. Zhou, *Joule*, 2020, **4**, 1743–1758.
- 3 M. Chen, S. R. Sahamir, G. Kapil, A. K. Baranwal, M. A. Kamarudin, Y. Zhang, K. Nishimura, C. Ding, D. Liu, D. Hirotsu, Q. Shen and S. Hayase, *Sol. Energy Mater. Sol. Cells*, 2020, **218**, 110741.
- 4 J. Lim, M. Kim, H. H. Park, H. Jung, S. Lim, X. Hao, E. Choi, S. Park, M. Lee, Z. Liu, M. A. Green, J. Seo, J. Park and J. S. Yun, *Sol. Energy Mater. Sol. Cells*, 2021, **219**, 110776.
- 5 X. Xia, W. Wu, H. Li, B. Zheng, Y. Xue, J. Xu, D. Zhang, C. Gao and X. Liu, *RSC Adv.*, 2016, **6**, 14792–14798.
- 6 M. Deepa, M. Salado, L. Calio, S. Kazim, S. M. Shivaprasad and S. Ahmad, *Phys. Chem. Chem. Phys.*, 2017, **19**, 4069–4077.
- 7 D. K. Maram, M. Haghighi, O. Shekoofa, H. Habibiyan and H. Ghafoorifard, *Sol. Energy*, 2021, **213**, 1–12.
- 8 E. Raza, Z. Ahmad, F. Aziz, M. Asif, A. Ahmed, K. Riaz, J. Bhadra and N. J. Al-Thani, *Sol. Energy*, 2021, **225**, 842–850.
- 9 J. Haddad, B. Krogmeier, B. Klingebiel, L. Krückemeier, S. Melhem, Z. Liu, J. Hüpkes, S. Mathur and T. Kirchartz, *Adv. Mater. Interfaces*, 2020, **7**, 2000366.
- 10 Y. H. Khattak, F. Baig, A. Shuja, S. Beg and B. M. Soucase, *Sol. Energy*, 2020, **207**, 579–591.
- 11 S. Karthick, J. Bouclé and S. Velumani, *Sol. Energy*, 2021, **218**, 157–168.